



ELSEVIER

Available online at [www.sciencedirect.com](http://www.sciencedirect.com)

Solar Energy Materials &amp; Solar Cells ■ (■■■■) ■■■-■■■

Solar Energy Materials  
and Solar Cells[www.elsevier.com/locate/solmat](http://www.elsevier.com/locate/solmat)

## Modeling the short-circuit current density of polymer solar cells based on P3HT:PCBM blend

Florent Monestier<sup>a</sup>, Jean-Jacques Simon<sup>a,\*</sup>, Philippe Torchio<sup>a</sup>, Ludovic Escoubas<sup>a</sup>, François Flory<sup>a</sup>, Sandrine Bailly<sup>b</sup>, Remi de Bettignies<sup>b</sup>, Stéphane Guillerez<sup>b</sup>, Christophe Defranoux<sup>c</sup>

<sup>a</sup>*Institut FRESNEL, UMR-CNRS 6133, Domaine Universitaire de St-Jérôme, 13397 Marseille Cedex 20, France*

<sup>b</sup>*INES CEADRTLITEN\DTSLCS, BP 332 50 av. du lac Léman 73370 Le Bourget du lac, France*

<sup>c</sup>*SOPRA-SA, Bois Colombes, France*

### Abstract

We have investigated the short-circuit current density of organic solar cells based on poly (3-hexylthiophene)(P3HT)/6,6-phenyl C61-butyric acid methyl ester (PCBM) blend. In order to model charge collection efficiencies with respect to short circuit density in such blends, a full optical modeling of the cell is performed. From the distribution of the electromagnetic field, we compute the rate of exciton generation. This exciton generation rate is used as input in the transport equations of holes and electrons. Charge densities at steady state are obtained as solutions are used for computing short-circuit current densities generated in the cell. The dependence of short-circuit current densities versus the thickness of the blend is analyzed and compared with our experimental data and with data extracted from the literature.

© 2006 Elsevier B.V. All rights reserved.

**Keywords:** Organic solar cells; Short-circuit density; Optical modeling; P3HT:PCBM blend

### 1. Introduction

Organic solar cells have been receiving increasing attention over the last few years. Indeed, the materials used in polymer photovoltaic field offer many practical advantages over conventional photovoltaic materials such as silicon due to the solution processing techniques used to fabricate the cells. Blend heterojunctions consisting of a bulk mixing of poly (3-hexylthiophene)(P3HT) as donor and 6,6-phenyl C61-butyric acid methyl ester (PCBM) as acceptor are very promising structures [1]. Power conversion efficiencies of organic photovoltaic cells based on P3HT:PCBM bulk heterojunctions up to 4.4% have been reported [2]. Studies on blend nanoscale morphology [3] and stability of organic solar cell [4] are the currently subjects of intense research. For example, an optimization parameter such as weight ratio between

donor and acceptor increases the number of donor/acceptor interfaces and reduces the distance leading to exciton dissociation at the interfaces, resulting in a high-exciton dissociation efficiency [5]. However, after dissociation, charges have to be collected at the electrodes through percolation pathways in the hole and electron transporting phases and the efficiency of the blend can be limited by charge recombinations at the interfaces of these phases [6]. The optical properties of organic thin film photovoltaic devices are substantially influenced by interference effects that contribute to the electromagnetic field modulation inside the device. We have developed a software that allows the computation of the electromagnetic field distribution in the depth of organic multi-layer structures under a polychromatic incoming irradiation with standard AM1.5 distribution ( $100 \text{ mW cm}^{-2}$ ). Lot of research works on thicknesses optimization based on optical modeling has been done [7,8] in order to increase light absorption inside active layers. Unfortunately, it is difficult to improve the photovoltaic efficiency

\*Corresponding author.

E-mail address: [jean-jacques.simon@fresnel.fr](mailto:jean-jacques.simon@fresnel.fr) (J.-J. Simon).

experimentally because even if the optical absorption increases the charge collection efficiency may decrease [9]. Therefore, we have to consider simultaneously optical and electrical effects. Consequently, we have developed a model considering a charge drift-diffusion current in order to calculate short-circuit current densities of organic solar cell. We wonder whether short-circuit current variations with increasing blend thickness could be predicted. The short-circuit current simulation of organic solar cells has recently been reported by several research groups. Lacic and Inganäs [10] have modeled the short-circuit current of a device consisting of a blend poly(2,7-(9-di-octyl-fluorene)-*alt*-5,5-(4',7'-di-2-thienyl-2',1',3'-benzothiadiazole))APFO3:PCBM. They calculated charge densities at steady state with optical modeling as input and boundaries conditions governed by charge injections. The model was used in order to investigate the role of transport parameters in device performance. Results indicate that the main effort should be put on reaching higher hole mobility, lower recombination and higher anode work function. Koster et al. [11] compared the photocurrent measurements of bulk heterojunction solar cells, consisting of a blend poly(2-methoxy-5-(3',7'-dimethyl-octyloxy)-*p*-phenylene vinylene) (MDMO-PPV):PCBM, with modeling of the bound electron-hole pair dissociation probability. Their results suggest bimolecular recombination to be a significant loss mechanism in photovoltaic devices, although weak at short circuit. Charge recombination in a blend of MDMO-PPV:PCBM as active layer has also been modeled by Nelson et al. [12]. The microscopic model is based on the multiple trapping of hole polarons in deep traps in the polymer. Their model allows the computation of the influence of intensity and temperature on short-circuit current. In our simulations, interference effects are taken into account inside the whole structure. In our model, from the distribution of the electromagnetic field, we compute the rate of exciton generation ( $G$ ). This exciton generation rate is used as input in the transport equations of holes and electrons because of the efficient ultrafast charge transfer from organic materials to fullerene derivatives [13]. Charge densities at steady state are obtained as solution and used for computing short-circuit current densities. The thickness dependence of short-circuit current densities is analyzed and compared with experimental data. In the case of no charge recombination, the optical modeling gives the value of the maximum photocurrent to be extracted from the cell. In the case of charge recombination, transport parameters are adjusted in order to understand typical behaviors in these materials. In the first part of this paper, we describe the numerical model while in a second part, we present the solar cell structure and its optical constants. We then give the generation rate distribution inside the blend and in a third part, we present charge densities and current profiles in the blend. In the last part, we study short-circuit current densities as a function of blend thickness and we compare it with the experimental data.

## 2. Model

To complete short-circuit current densities analysis, we have to calculate charge densities at steady state taking into account the transport properties such as drift and diffusion of holes and electrons. Thus, charge continuity equation (Eq. (1)) has to be solved [14],

$$\frac{1}{q} \frac{dJ(z)}{dz} + G(z) - R(z) = 0. \quad (1)$$

At each point  $z$  in the depth of the blend, the short-current density  $J(z)$  is the difference between the generation rate of free carriers  $G(z)$  and the recombination rate  $R(z)$ . In organic solar cells, the incoming light generates excitons inside the blend due to electron transitions from the highest occupied molecular orbital (HOMO) to for the lowest unoccupied molecular orbital (LUMO) bands. Assuming that the exciton dissociation rate is equal to 1,  $G(z)$  only depends on the number of photons absorbed per second in the active layer. Recombination losses in bulk-heterojunction solar cells have been widely studied and two recombination mechanisms are usually distinguished: first-order recombination and bimolecular recombination. The first-order recombination depends on trap densities (due to the presence of impurities such as oxygen in the blend) and is defined in the case of electrons by  $R = n/\tau$ , where  $\tau$  is the electron lifetime and  $n$  is the electron density. The bimolecular recombination rate depends on charge densities of holes and electrons and is defined by  $R = Kpn$ , where  $p$  is the hole density and  $K$  is the bimolecular coefficient. The problem is studied in one dimension along the  $z$ -axis perpendicular to the surface plane. The blend is supposed to be a homogenous medium in which hole and electron can move independently through percolation pathways. The drift-diffusion equation is given by [15]

$$J_n = J_{\text{diffusion}} + J_{\text{drift}} = qD_n \frac{dn(z)}{dz} + \mu_n q E(z)n(z), \quad (2)$$

where  $D_n$  is the electron diffusion coefficient defined by the Einstein relation,  $\mu_n$  is the electron mobility and  $n(z)$  is the electron density. The electric field  $E(z)$  in Eq. (2) is assumed to be constant and defined by  $E = V_{\text{bi}}/e$ , where  $V_{\text{bi}}$  is the built-in potential and  $e$  is the blend thickness. The same Eqs. (1) and (2) hold for holes. From Eq. (1), the charge generation rate  $G(z)$  is needed to determine charge densities at equilibrium. We refer to previous work for a more detailed description of the theory concerning device modeling [16]. The electromagnetic field in organic solar cells is numerically calculated. Interference effects are taken into account inside the whole structure. The local energy dissipated in the material at a depth point  $z$  for a wavelength  $\lambda$ ,  $Q(z, \lambda)$ , is calculated according to the Poynting formula:  $\mathbf{Q} + \text{div}(\mathbf{P}) = 0$ , where  $\mathbf{P} = \frac{1}{2}(\mathbf{E} \times \mathbf{H}^*)$ . Then,  $Q$  in a layer  $i$  is given versus the depth  $z$  and the

wavelength  $\lambda$  by

$$Q(z, \lambda) = \frac{1}{2} \sqrt{\frac{\varepsilon_0}{\mu_0}} n_i \alpha |E(z)|^2 = \frac{n_i}{n_0} \alpha I_{\text{solar light}} \left| \frac{E(z)}{E_0} \right|^2, \quad (3)$$

where  $\varepsilon_0$  is the vacuum permittivity and  $\mu_0$  is the vacuum permeability,  $\alpha$  is the absorption coefficient,  $n_i$  and  $n_0$ , are respectively, the real part of the complex refractive index of the layer  $i$  and of the substrate, and  $I_{\text{solar light}}$  is the polychromatic incoming light with standard AM1.5 distribution ( $100 \text{ mW cm}^{-2}$ ). The unit of the dissipated energy  $Q(z, \lambda)$  is  $\text{W m}^{-2} \text{ nm}^{-1}$ . Then, we divide the energy dissipated  $Q(z, \lambda)$  by the incoming energy and we obtain the  $G(z, \lambda)$  number of photons dissipated per second as function of depth and wavelength:

$$G(z, \lambda) = \frac{Q(z, \lambda)}{h\nu}. \quad (4)$$

Finally, the sum of  $G(z, \lambda)$  on all the visible spectrum is done and we obtained the photon generation rate at a  $z$  depth point:

$$G(z) = \sum_{\lambda=300}^{900} G(z, \lambda). \quad (5)$$

Assuming the rate of exciton dissociation into charge carriers to be unity, the rate of exciton generation equals the carrier generation rate. Boundary conditions play an important role because they may considerably affect the distribution of charge densities at the interfaces. It is possible to fix boundary conditions considering charge or current densities. We choose boundary values on current densities. Boundary conditions are set in order to have no hole current at the cathode and no electron current at the anode. The previous equations are solved on a discrete grid using a linear algebra package [17]. After solving ordinary differential equation system with boundary values, we obtain the charge densities in the device at steady state.

### 3. Experimental

All the bulk heterojunction photovoltaic cells were prepared from a solution of P3HT:PCBM at 1:1 weight ratio. The glass-ITO substrates (obtained from PGO<sup>®</sup>, Germany) were sequentially cleaned in an ultrasonic bath by using acetone and isopropanol, then rinsed with deionized water, dried in an oven at  $120^\circ\text{C}$  during 30 min and finally treated with UV generated ozone. The substrates were then spin coated with poly(3,4-ethylenedioxythiophene)-blend-poly(styrene-sulfonate)(PEDOT:PSS) (Baytron PH<sup>®</sup>) at 1500 rpm, and oven dried for 30 min at  $120^\circ\text{C}$  to obtain a 50 nm thick film. The active P3HT:PCBM layer was deposited by spin casting from an anhydrous chlorobenzene solution under dry nitrogen.

Following drying under reduced pressure at  $2 \times 10^{-7}$  mbar for 1 h, the devices were completed by deposition of the LiF/Al (0.8 and 100 nm thick, respectively) cathode through a shadow mask. All the cells have a  $28 \text{ mm}^2$  active surface and blend thicknesses are varied between 30 and 215 nm. The annealing process was carried out under an inert atmosphere by placing the cells or films deposited on glass directly onto a controlled hot plate. Cell performances were evaluated following free cooling to ambient temperature. Current–voltage characteristics and power conversion efficiencies of the solar cells were measured in an inert atmosphere via a computer controlled Keithley<sup>®</sup> SMU 2400 unit using  $100 \text{ mW cm}^2$  air-mass (1.5) simulated white light developed by a Steuernagel solar constant 575 simulator.

## 4. Simulation results and comparison with experimental data

### 4.1. Current density profiles in the blend

Optical constants ( $n, k$ ) of each layer (ITO, PEDOT and active layer) have been determined by ellipsometric measurements and used as input parameters in our software. Layer thicknesses were experimentally determined by using a mechanical profilometer. Optical constants of P3HT:PCBM blends are shown in Fig. 1. The absorption domain ranges between  $\lambda = 300$  and 650 nm. We compute the energy dissipated inside the active area taking into account the interference effects. Profiles of exciton generation rate for various blend thicknesses are shown in Fig. 2. We note the modulations of exciton generation rate with thickness variations. The hole and electron mobilities are taken from literature: Hole mobility in P3HT and electron mobility in PCBM, are respectively,  $2 \times 10^{-8}$  and  $3 \times 10^{-7} \text{ m}^2 \text{ V}^{-1} \text{ s}^{-1}$  at 300 K [18]. We consider that charge mobility values in blend are similar to those in pure materials, even if hole mobility in blend is expected to be lower. The built-in potential ( $V_{\text{bi}}$ ), which is the

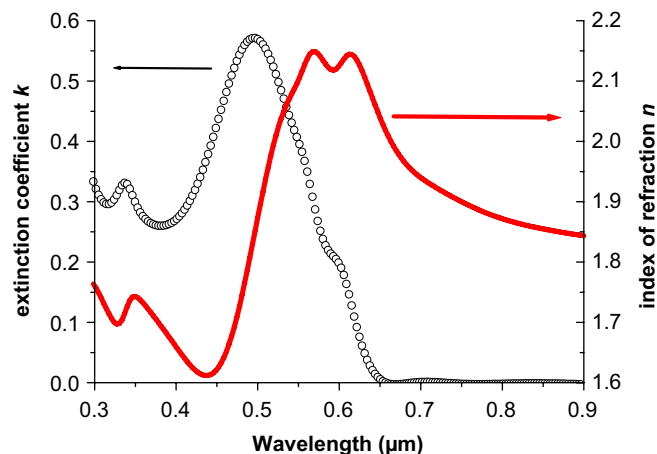


Fig. 1. Optical index  $n(\lambda)$  (solid line) and extinction coefficient  $k(\lambda)$  (circle) of the blend P3HT:PCBM at 1:1 weight ratio (spectrometric ellipsometry measurement).

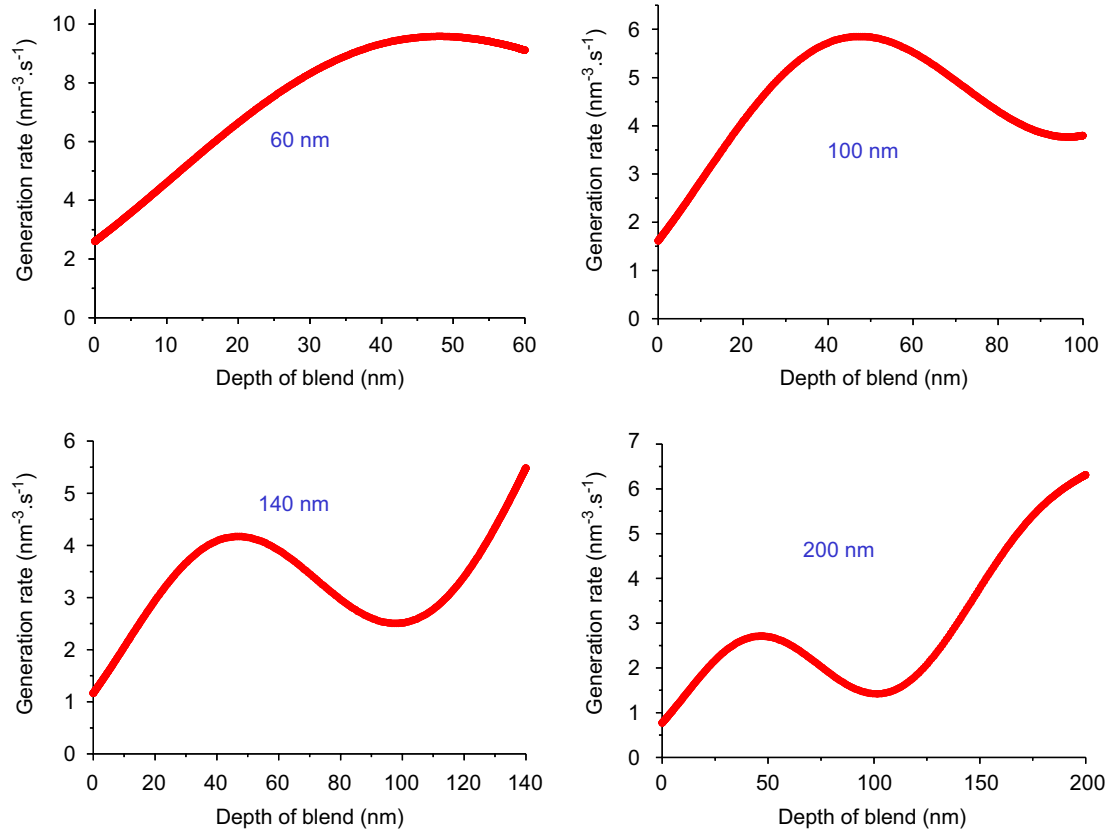


Fig. 2. Profiles of exciton generation rate for various blend thicknesses (60, 100, 140, and 200 nm)

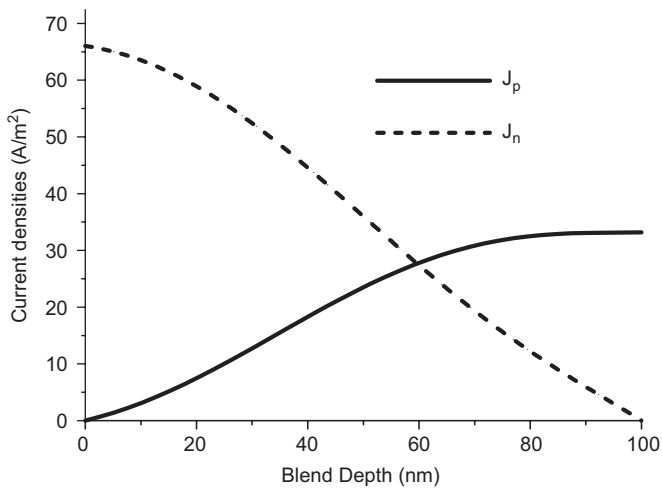


Fig. 3. Current densities ( $J_n$  for electrons and  $J_p$  for holes) versus blend depth computed using first-order recombination ( $\tau_n = 2 \times 10^{-7}$  s and  $\tau_p = 1 \times 10^{-6}$  s).

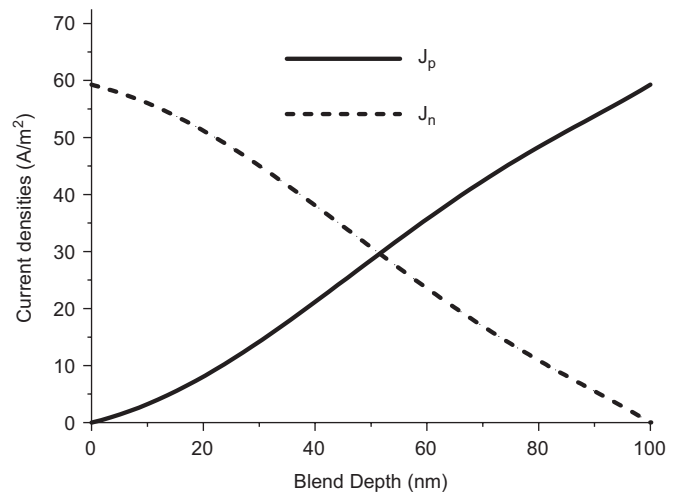


Fig. 4. Current densities (electrons dashed line—holes solid line) versus blend depth. Computation using bimolecular recombination ( $K = 3 \times 10^{-13}$  m<sup>3</sup> s<sup>-1</sup>).

difference between cathode and anode work functions, is taken equal to 0.7. After solving transport equation, we obtain charge densities and short-circuit current density distribution at steady state. We assume the current not to be limited by space charges and the effect of photoinduced charge carriers on the field distribution to be negligible.

Current densities as a function of blend depth are computed using first-order recombination (Fig. 3).

As expected, the hole current density is higher on the ITO anode side and the electron current density is higher on the aluminum cathode side. Values at the opposite contacts are null and the decrease of current densities is monotonous which is not surprising as the electric field is

constant. Finally, the short-circuit current density is limited by the hole current density because hole mobility is one order lower than electron mobility. Current density distributions in the blend can also be computed from bimolecular recombination. As an example current densities versus the blend thickness are presented in Fig. 4.

#### 4.2. Short-circuit current densities versus blend thickness

In order to study the variation of short-circuit current as a function of blend thickness we realized and characterized 12 cells for each thickness. The cell structure is: ITO (180 nm)/PEDOT (45 nm)/blend P3HT:PCBM (1/1)/(various thicknesses)/Lif (1 nm)/Al (100 nm). Blend thicknesses are varied between 30 and 215 nm and short-circuit measurements are performed. Experimental measurements are plotted in Fig. 5. The experimental short-circuit current reaches its maximum value for a blend thickness of about 70 nm, followed by a little decrease until a 140 nm blend thickness and a new increase for thickness higher than 140 nm. This variation follows the optical energy absorption versus the blend thickness. This indicates that the recombination term is not necessary and could be suppressed in our computations. Values of lifetime and recombination coefficient were tuned in order to fit experimental data. A very high average lifetime or a very small bimolecular recombination coefficient was found to give the best fit. Comparison between experimental data and computation is shown in Fig. 5. We note a little deviation between simulated and experimental data for blend thicknesses higher than 180 nm. This deviation could be attributed to the thickness dependence of optical constants ( $n$ ,  $k$ ). Complementary studies of optical constants on a larger blend thickness range seems to be necessary. Moreover, this simulation indicates that carriers are collected at their respective electrodes without losses.

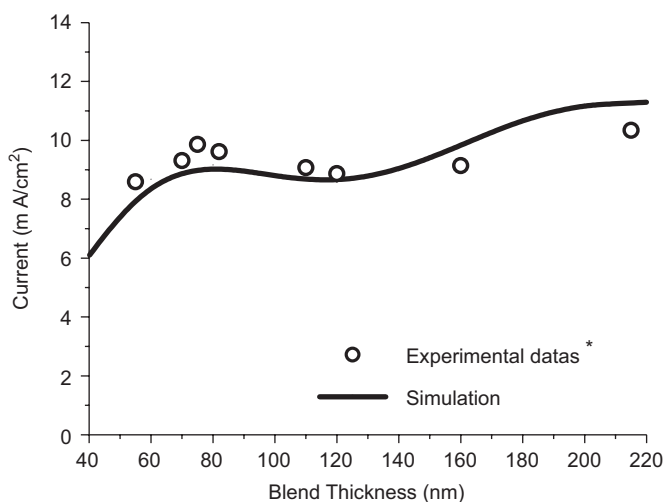


Fig. 5. Comparison of computed short-circuit current density (solid line) with experimental data (circles) as a function of blend thickness.

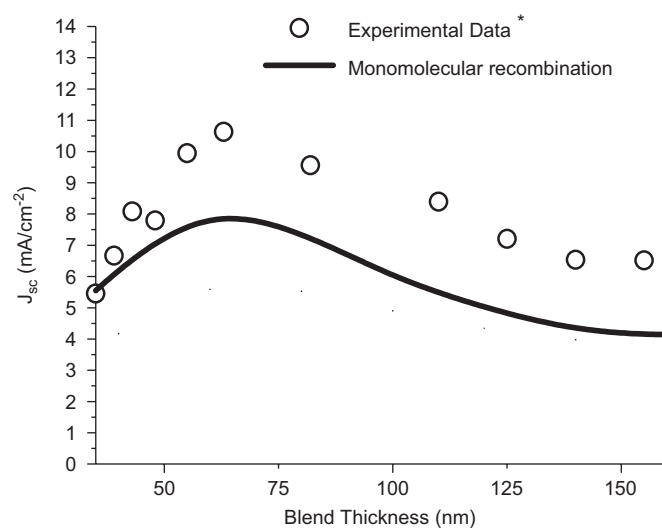


Fig. 6. Comparison of short circuit current density computations (solid line) and experimental data extracted from Ref. [19] (circle line) as function of the blend thickness.

Besides the intrinsic properties of P3HT and PCBM, our results suggest that the morphology of the blends presented in this work combine a phase separation at the nanometric scale that leads to increase the exciton dissociation and a crystalline order which improves charge transport. To verify if this particular behavior is related to the properties of our P3HT/PCBM blend, we have compared our computations with results from Li et al. [19], who have reported a study of the short-circuit current variations versus the P3HT:PCBM blend thickness. The authors have used a similar experimental procedure except for the thermal annealing conditions. Experimental short-circuit current extracted from Ref. [19] is plotted in Fig. 6 where blend thickness are varied between 35 and 155 nm. In this study, the maximum value of short-circuit current is higher, near 11 mA by  $\text{cm}^2$  for a 70 nm blend thickness, but instead of following exciton generation profile, the short-circuit current falls down by more than 40% for blends thicker than 100 nm. We assume that the optical indices of the blends investigated by Li et al. were the same as P3HT:PCBM blend and we perform simulation of  $J_{sc}$ . The computed curve is shown in Fig. 6. We obtain a better fit with first-order recombination than with bimolecular recombination. With an average hole lifetime  $\tau$  of 1.5  $\mu\text{s}$ , we observe the same decrease of the short-circuit current for thicker layers but with a vertical shift of 2 mA. In summary, we have simulated two types of  $J_{sc}$  behaviors: one with an increase of  $J_{sc}$  with blend thickness (for our P3HT:PCBM blend) and the other one with a decrease of  $J_{sc}$  (for P3HT:PCBM blend made by Li et al.). These differences could be related to optical and/or electrical properties of blend layers. Indeed, it has been widely demonstrated [20] that bulk heterojunction morphologies strongly depend on preparation conditions (such as purity of the material and thermal treatment).

## 5. Conclusion

We have shown that our computations, taking into account optical interferences, allows the prediction of the short-circuit current  $J_{sc}$  of bulk heterojunction organic solar cells. The P3HT:PCBM blend thickness dependence of short-circuit current densities was analyzed and compared with experimental data. It was found that the influence of the carrier recombination with  $J_{sc}$  variations depends on the experimental procedure. Even if short-circuit current densities increase with higher blend thicknesses, power conversion efficiency is usually limited by low fill factor. New simulations to explain the decrease of fill factor for thick layers are in progress.

## Acknowledgments

The authors acknowledge Agence Nationale pour la Recherche (ANR) for research funding under the solar photovoltaic program NANORGYSOL (ANR-05-PV-008-20).

## References

- [1] C.J. Brabec, Sol. Energy Mater. Sol. Cells 83 (2004) 273.
- [2] G. Li, V. Shrotriya, J. Huang, Y. Yao, T. Moriarty, K. Emery, Y. Yang, Nat. Mater. 4 (2005) 864.
- [3] H. Hoppe, T. Glatzel, M. Niggemann, W. Schwinger, F. Schaeffler, A. Hinsch, M.Ch. Lux-Steiner, N.S. Sariciftci, Thin Solid Films 511–512 (2006) 587.
- [4] R. De Bettignies, J. Leroy, M. Firon, C. Sentein, Synth. Metals 156 (2006) 510.
- [5] T. Martens, J. D’Haen, T. Munters, Z. Beelen, L. Goris, J. Manca, M. D’Olieslaeger, D. Vanderzande, L. De Schepper, R. Andriessen, Synth. Met. 138 (2003) 243.
- [6] G. Dennler, A.J. Mozer, G. Juska, A. Pivrikas, R. Osterbacka, A. Fuchsbaauer, N.S. Sariciftci, Org. Electron. 7 (2006) 229.
- [7] N.-K. Persson, M. Schubert, O. Inganäs, Sol. Energy Mater. Sol. Cells 83 (2004) 169.
- [8] D.P. Gruber, G. Meinhardt, W. Papousek, Sol. Energy Mater. Sol. Cells 79 (2005) 697.
- [9] N.-K. Persson, H. Arwin, O. Inganäs, J. Appl. Phys. 97 (2005) 034503.
- [10] S. Lacic, O. Inganäs, J. Appl. Phys. 97 (2005) 124901.
- [11] L.J.A. Koster, E.C.P. Smits, V.D. Mihailetchi, P.W.M. Blom, Phys. Rev. B 72 (2005) 085205.
- [12] J. Nelson, S.A. Choulis, J.R. Durrant, Thin Solid Films 451–452 (2004) 508.
- [13] B. Kraabel, D. McBranch, N.S. Sariciftci, D. Moses, A.J. Hegger, Phys. Rev. B 50 (24) (1994) 18543.
- [14] D. Vacar, E.S. Malinoff, W.D. McBranch, A.J. Hegger, Phys. Rev. B 56 (8) (1997) 4573.
- [15] A. Vapaille, Dispositifs et circuits intégrés semiconducteurs, Dunod, Paris, 1990.
- [16] F. Monestier, P. Torchio, J.J. Simon, L. Escoubas, M. Cathelinaud, Non linear optics and quantum optics, to be published.
- [17] Matlab (The Mathworks Inc.), Natick, MA.
- [18] V.D. Mihailetchi, H. Xie, B. de Boer, L.J.A. Koster, P.W.M. Blom, Adv. Funct. Mater. 16 (2006) 699.
- [19] G. Li, V. Shrotriya, Y. Yao, Y. Yang, J. Appl. Phys. 98 (2005) 043704.
- [20] X. Yang, J. Loos, S.C. Veenstra, W.J.H. Verhees, M.M. Wienk, J.M. Kroon, M.A.J. Michels, R.A.J. Janssen, Nano. Lett. 5 (4) (2005) 579.